



TITLE:

The Role of Granule Size on the Kinetics of Electrochemical Reduction of SiO₂ Granules in Molten CaCl₂

AUTHOR(S):

Yang, Xiao; Yasuda, Kouji; Nohira, Toshiyuki;
Hagiwara, Rika; Homma, Takayuki

CITATION:

Yang, Xiao ...[et al]. The Role of Granule Size on the Kinetics of Electrochemical Reduction of SiO₂ Granules in Molten CaCl₂. Metallurgical and Materials Transactions B: Process Metallurgy and Materials Processing Science 2016, 47(1): 788-797

ISSUE DATE:

2016-02

URL:

<http://hdl.handle.net/2433/230381>

RIGHT:

This is a post-peer-review, pre-copyedit version of an article published in 'Metallurgical and Materials Transactions B'. The final authenticated version is available online at: <https://doi.org/10.1007/s11663-015-0456-1>; The full-text file will be made open to the public on 1 February 2017 in accordance with publisher's 'Terms and Conditions for Self-Archiving'; この論文は出版社版ではありません。引用の際には出版社版をご確認ご利用ください。; This is not the published version. Please cite only the published version.

The Role of Granule Size on the Kinetics of Electrochemical Reduction

of SiO₂ Granules in Molten CaCl₂

Xiao Yang^a, Kouji Yasuda^{b,c}, Toshiyuki Nohira^a, Rika Hagiwara^b, and Takayuki Homma^d

^aInstitute of Advanced Energy, Kyoto University, Gokasho, Uji, Kyoto 611-0011, Japan

^bGraduate School of Energy Science, Kyoto University, Yoshida-honmachi, Sakyo-ku, Kyoto 606-8501, Japan

^cEnvironment, Safety and Health Organization, Kyoto University, Yoshida-honmachi, Sakyo-ku, Kyoto 606-8501, Japan

^dFaculty of Science and Engineering, Waseda University, 3-4-1 Okubo, Shinjuku-ku, Tokyo 169-8555, Japan

Corresponding authors:

X. Yang (yang.xiao.6a@kyoto-u.ac.jp)

T. Nohira (nohira.toshiyuki.8r@kyoto-u.ac.jp)

Abstract

As a fundamental study to develop a new process for producing solar-grade silicon, the effect of granule size on the kinetics of the electrochemical reduction of SiO_2 granules in molten CaCl_2 was investigated. SiO_2 granules with different size ranges were electrolyzed in molten CaCl_2 at 1123 K (850 °C). The reduction kinetics was evaluated on the basis of the growth rate of the reduced Si layer and the behavior of the current during electrolysis. The results indicated that finer SiO_2 granules are more favorable for a high reduction rate because the contact resistance between the bottom Si plate and the reduced Si particles is small and the diffusion of O^{2-} ions in CaCl_2 inside the porous Si shell is easy. Electrolysis using SiO_2 granules less than 0.1 mm in size maintained a current density of no less than 0.4 A cm^{-2} within 20 min, indicating that the electrochemical reduction of fine SiO_2 granules in molten CaCl_2 has the potential of becoming a high-yield production process for solar-grade silicon.

I. INTRODUCTION

The global photovoltaic (PV) market has been growing rapidly in recent years. In 2013, the annual installation of PV systems in the world reached 37 GW,^[1] which was a 60-fold increase as compared to 2003. Yet the power globally generated from solar energy was less than 0.5 pct of the total power generation in 2012.^[2] According to a study by the German Advisory Council on Global Change (WBGU), solar energy is expected to become a major energy source, reaching 20 pct of the total world energy by 2050 and 70 pct by 2100.^[3] Presently, the dominant material for solar cells is silicon, particularly crystalline silicon. Crystalline silicon solar cells represented 90.1 pct of the global production of all types of solar cells in 2013.^[4] Because they offers advantages in terms of high conversion efficiency, high durability, non-toxicity, and abundant resources, silicon solar cells are the only candidate to meet the market demand in the future when PV installation could climb to several hundred GW per year.

The increasing demand for PV systems boosts the production of high-purity polycrystalline Si dramatically. The global production of polycrystalline Si in 2013 saw a 10-fold increase since 2003 to 233,800 t,^[5] more than 90 pct of which was supplied to the PV industry. Such growth is expected to continue over the long term. For PV applications, the purity of Si must be at least 6N (99.9999 pct), and this product is called solar-grade Si (SOG-Si). The dominant technology for SOG-Si production is the Siemens process,^[6-8] which represents approximately 90 pct of the global

production. In spite of the ability to produce Si at purity levels above 9N, the Siemens process, which utilizes chemical vapor deposition using trichlorosilane (SiHCl_3), requires high energy consumption and results in low productivity. Production of SOG-Si based on pyrolysis of monosilane (SiH_4) in a fluidized bed reactor (FBR) is the main competitor to the Siemens process and represents about 10 pct of the market.^[8-10] FBR consumes less energy and it is more economical than the Siemens process, yet limitations in terms of purity control and productivity inhibit its commercial application. Upgrading metallurgical-grade silicon (UMG) is an emerging process for SOG-Si production. The aim of this process is to cost-effectively refine metallurgical-grade Si by slag treatment, acid leaching, and directional solidification.^[11-13] However, UMG has a relatively small market share at present because of problems with purity control.^[8,14] Various attempts have been made to optimize the present technologies to improve energy efficiency and productivity and to reduce cost.^[15-20] Meanwhile, new SOG-Si production processes^[21-22] such as the carbothermic reduction of silica using high-purity raw materials,^[23] refining of metallurgical-grade Si by different approaches,^[24-32] metallothermic reduction of silicon compounds,^[33-40] and electrochemical processes,^[41-48] are being developed to challenge the existing technologies.

Electrochemical reduction of solid oxides in molten salt has been widely studied since it was firstly reported by Fray and his colleagues.^[49-57] We originally demonstrated that solid silica (SiO_2) can be electrochemically reduced to solid Si in molten salts via the solid-to-solid reaction:^[58-71]



69 Similar works have been reported by other researchers.^[72-84] Chen and his colleagues^[72-75] studied
70 the reduction behavior of SiO₂ plates or pellets in molten CaCl₂ based on electrochemical
71 measurements. We came up with a novel idea for SOG-Si production by combining direct
72 electrochemical reduction with the use of high-purity silica, acid leaching, and directional
73 solidification.^[64] Impurities in the Si produced by this method were experimentally demonstrated to
74 be at a low level.^[68] A semi-continuous electrochemical reduction process was thus proposed,^[69] in
75 which SiO₂ granules as the raw material supplied from the top side of the electrolysis cell are
76 reduced at the cathode placed at the bottom and recovered as slurry containing molten CaCl₂. The
77 kinetic characteristics of the reducing process of SiO₂ granules were clarified by measuring the
78 weight change of the samples during electrolysis.^[70] The apparent current density was 0.7 A cm⁻² at
79 the initial stage of electrolysis, which indicates the promise of this process in terms of productivity.

80 An integrated understanding of the mechanism and kinetics of the direct electrochemical reduction
81 of solid SiO₂ in a molten salt is crucial for upscaling of the laboratory experiment to commercial
82 production. In our previous study, we systematically investigated the reduction behavior of SiO₂
83 granules on a bottom cathode in molten CaCl₂ at 1123 K (850 °C) by visually observing changes to
84 the reaction interfaces after different electrolysis durations.^[71] The overall reduction was found to

85 proceed via two different routes: (1) from the SiO_2 granules near the conductor to the distant
86 granules along the granule surfaces and (2) from the surface to the core in each partly reduced
87 granule. Formation of a core (SiO_2)–shell (Si) structure for partly reduced SiO_2 granules indicated
88 that the reduction along the granule surfaces was faster than that from the surface to the core. On the
89 basis of such findings, finer SiO_2 granules are expected to be more favorable for a high reduction
90 rate owing to the larger surface area. However, this expectation needs to be experimentally
91 confirmed.

92 High productivity is crucial for every practical production process for SOG-Si, including molten
93 salt electrolysis. In this process, the size of SiO_2 granules is considered to be one of the key
94 parameters that strongly affects the reduction kinetics and thus determines the productivity.
95 Therefore, the purpose of the present study was to clarify the effect of granule size on the kinetics of
96 the electrochemical reduction of SiO_2 granules in molten CaCl_2 . SiO_2 granules with different size
97 ranges were electrolyzed in molten CaCl_2 at 1123 K (850 °C). The reduction kinetics was
98 quantitatively evaluated in terms of both the growth rate of the reduced layer and the behavior of the
99 current during electrolysis. A reaction model that illustrates the reduction process and the
100 dependence of reduction kinetics on granule size is proposed.

II. EXPERIMENTAL

A. Materials and Apparatus

Approximately 400 g of CaCl_2 (Kojundo Chemical Lab. Co., Ltd., 99 pct) was used as the electrolyte bath. Prior to use, the CaCl_2 was dried under vacuum at 453 K (180 °C) for 72 h and 773 K (500 °C) for 24 h to remove the residual moisture. Approximately 0.13 g of SiO_2 granules (Kojundo Chemical Lab. Co., Ltd., 99 pct) in four size ranges (less than 0.1 mm, 0.10–0.25 mm, 0.5–1.0 mm, and 1.0–2.0 mm), shown in Figure 1, were used in this study. These granules were obtained from large granules (2.0–5.0 mm) after grinding and screening.

***** Figure 1 *****

Figure 2(a) shows a schematic of the electrolysis cell. An Al_2O_3 crucible (Nikkato Corp., o.d. 90 × i.d. 80 × height 100 mm) charged with CaCl_2 was set inside a SiO_2 vessel and heated to 1123 K (850 °C) in a dry Ar atmosphere (100 mL min⁻¹). The working electrode (WE) comprised an Al_2O_3 tube (Nikkato Corp., o.d. 8 × i.d. 5 × height 15 mm) and a Si plate [Nilaco Corp., diameter 10.0 × thickness 0.5 mm, n-type, (100) plane], which served as a container and a current collector respectively, as shown in Figure 2(b). SiO_2 granules were charged in the Al_2O_3 tube. A nickel wire (Nilaco Corp., diameter 1.0 mm, 99 pct) used as the current lead was connected to the Si plate by threading it into a drilled hole (diameter 1.1 mm). With this setup, electrical contact to the SiO_2 occurred only through the Si plate at the bottom of the Al_2O_3 tube.

***** Figure 2 *****

The counter electrode (CE) was a glassy carbon rod (Tokai Carbon Co., Ltd., diameter 5.2 mm). The reference electrode (RE) was an Ag^+/Ag electrode prepared by immersing a silver wire (Nilaco Corp., diameter 1.0 mm, 99 pct) into CaCl_2 containing 0.5 mol pct AgCl (Wako Pure Chemical Co., Ltd., 99.5 pct) in a mullite tube (Nikkato Corp., o.d. $6 \times$ i.d. $4 \times$ height 450 mm).^[63] A molybdenum wire (Nilaco Corp., diameter 1.0 mm, 99 pct) was used to conduct the cyclic voltammetry to calibrate the Ca^{2+}/Ca potential and check the potential of the Ag^+/Ag reference electrode.

B. Procedure

After conducting the cyclic voltammetry using the Mo wire to calibrate the Ca^{2+}/Ca potential, the potential of the working electrode was set at 0.5 V vs. Ca^{2+}/Ca for the potentiostatic electrolysis for 10–100 min. The working electrode was immediately taken out from the melt after electrolysis and a new one was immersed for another run. The post-electrolysis working electrode was cut vertically into two halves to observe the cross section. In some cases, the post-electrolysis working electrode was washed in 10 M HCl (aq.) for 3 h to disassemble the Si plate at the bottom. The upper surface of the Si plate in contact with the SiO_2 granules was observed.

III. RESULTS

A. Contact of SiO_2 Granules with the Bottom Si Plate

Figure 3 compares the appearance of the upper surface of the bottom Si plate after electrolysis for 10 min using SiO₂ granules of different size ranges, as well as that of a blank test with no SiO₂ granules. In the case of the blank test [Figure 3(e)], the surface was essentially smooth and integrated. When using SiO₂ granules less than 0.1 mm in size [Figure 3(a)], some parts of the surface were broken, and a large amount of reduced Si, which appears brown in the figure, was attached to the surface. This result indicates that the reduced Si and the bottom Si plate were in close contact with each other during electrolysis. The broken surface was caused by disassembling the Si plate from the post-electrolysis electrode. Since the crystallization rate for amorphous Si increases with increasing temperature and reaches 1 μm s⁻¹ at 1123 K (850 °C),^[85] the reduced Si, which was amorphous immediately after its formation, might have rapidly crystallized and sintered to have the same orientation as the bottom Si plate. In the case of SiO₂ granules 1.0–2.0 mm in size [Figure 3(d)], only a small amount of reduced Si was found on the surface. In Figures 3(a)–(d), it can be noticed that the quantity of attached Si and broken areas are decreasing and the surface becomes more integrated with increasing SiO₂ granule size. This trend indicates that the contact of SiO₂ granules with the bottom Si plate was improved by decreasing the granule size.

***** Figure 3 *****

B. Growth of the Reduced Si Layer

Figure 4 shows the cross sections of the working electrodes using SiO₂ granules with different

size ranges after electrolysis for (I) 20 min and (II) 60 min at 0.5 V vs. Ca^{2+}/Ca in molten CaCl_2 at 1123 K (850 °C). For each sample, a dark brown layer is observed above the Si plate at the bottom. Formation of crystalline Si in this layer was confirmed by X-ray diffraction (XRD) and scanning electron microscopy/energy dispersive X-ray spectroscopy (SEM/EDX). A downward shift of unreduced SiO_2 granules was not observed in Figure 4, indicating that the granules piled on the Si plate as a whole did not apparently shrink downward after reduction. The thickness of the dark layer at three positions in each cross section was measured using a ruler. The average thicknesses of the reduced layers are plotted against electrolysis time in Figure 5. The increased thickness from 20 min to 100 min indicates the propagation of the reduction from the bottom of the SiO_2 layer to the top. Faster growth of the reduced layer was observed for the smaller granules, indicating a larger reduction rate.

***** Figure 4 *****

***** Figure 5 *****

C. Behavior of the Current

Figure 6 shows typical current transient curves during electrolysis for 20 min using SiO_2 granules in the various size ranges. The current was larger at the beginning, and it gradually decreased as the electrolysis progressed. A larger current was observed for the smaller granules, indicating a faster reduction rate. Figure 6(e) shows the current of a blank electrolysis test for 10 min using the same

working electrode without a charge of SiO_2 granules. The detected background current is probably due to the side electrochemical reactions of the residual moisture in the molten salt. In this study, the background current was assumed to be independent of the electrolysis time and charge of SiO_2 granules. The effective current corresponding to SiO_2 reduction was considered to be the difference between the measured current and the background current, as indicated in Figure 6.

***** Figure 6 *****

IV. DISCUSSION

A. Effect of Granule Size on Contact Resistance

Figure 3 shows that contact between the SiO_2 granules and the bottom Si plate can be improved by decreasing the granule size. Such a difference is schematically illustrated in Figure 7. Assuming the granules are perfectly spherical in shape, the number of contact points equals the number of granules in direct contact with the Si plate (N_I), which can be calculated by

$$N_I = \frac{A_{\text{plate}}}{\pi r_0^2} \quad (2)$$

where A_{plate} is the geometrical area of the Si plate and r_0 is the granule radius. Apparently, small granules guarantee a larger number of contact points and thus a greater total contact area as compared with the large granules.

***** Figure 7 *****

As reduction proceeds along the granule surface and from the granule surface to the core, the reduction front gradually moves away from the initial point and spreads along the unreduced part of the SiO_2 granule.^[71] The effective potential at the reduction front is determined by the contact resistance between the bottom Si plate and the reduced part of the SiO_2 granules.^[73] Because the reduction kinetics is favored at more negative potentials,^[61] the usage of small granules guarantees a lower potential drop, thus improving the reduction kinetics.

B. Reaction Model for the Reduction during Electrolysis

Figure 8 illustrates the reduction of the SiO_2 granules piled on the Si plate based on our previous study.^[71] A reaction model is proposed to explain the reduction at three stages of electrolysis with the following assumptions: the SiO_2 granules are perfectly spherical in shape; the effective area for each contact point between SiO_2 granule and Si plate is the same and independent of granule size; the granules never expand or shrink during electrolysis; the Si shell formed at the beginning of electrolysis is of an infinitesimal thickness that remains constant over short time periods; the diffusion coefficients of O^{2-} ions in CaCl_2 at the granule surface and inside the granule are independent of granule size; partly reduced granules after electrolysis for large time t have an identical geometry; and the concentration of O^{2-} ions changes linearly in CaCl_2 in the crevices of the Si shells from inside to outside.

***** Figure 8 *****

209 At the start of the electrolysis (infinitesimal time t), reduction occurs at the contact points between
210 SiO_2 granules and the Si plate, as shown in Figure 8(a). Since diffusion of O^{2-} ions in CaCl_2 is the
211 rate-determining step for the reduction, from Fick's first law of diffusion, the reduction rate at this
212 moment ($\dot{n}_{\text{Si}}^{t \rightarrow 0}$) can be described by

$$213 \quad \dot{n}_{\text{Si}}^{t \rightarrow 0} = \frac{\dot{n}_{\text{O}^{2-}}}{2} = \frac{-1}{2} N_I A_{\text{cont.}} D_{\text{surf.}} \left(\frac{dC_{\text{O}^{2-}}}{dr} \right)_{\text{surf.}} = \frac{-A_{\text{plate}}}{2\pi r_0^2} A_{\text{cont.}} D_{\text{surf.}} \left(\frac{dC_{\text{O}^{2-}}}{dr} \right)_{\text{surf.}} \quad (3)$$

214 Where $\dot{n}_{\text{O}^{2-}}^{t \rightarrow 0}$ is the formation rate of O^{2-} ions at the start of the electrolysis, $A_{\text{cont.}}$ is the effective area
215 for each contact point, and $D_{\text{surf.}}$ and $\left(\frac{dC_{\text{O}^{2-}}}{dr} \right)_{\text{surf.}}$ are the diffusion coefficient and concentration
216 gradient of O^{2-} ions in CaCl_2 at the granule surface, respectively. Since A_{plate} is constant and $A_{\text{cont.}}$,
217 $D_{\text{surf.}}$, and $\left(\frac{dC_{\text{O}^{2-}}}{dr} \right)_{\text{surf.}}$ are considered to be independent of granule size, Eq. [3] indicates that the
218 reduction rate at the start of electrolysis decreases with increasing granule radius.

219 With increasing t , reduction proceeds upward along the granule surface and from surface to core
220 with the formation of a Si shell, as shown in Figure 8(b-1). The overall reduction rate ($\dot{n}_{\text{Si}}^{\text{overall}}$) can
221 be expressed as

$$222 \quad \dot{n}_{\text{Si}}^{\text{overall}} = \dot{n}_{\text{Si}}^{\text{surf.}} + \dot{n}_{\text{Si}}^{\text{ins.}} \approx \dot{n}_{\text{Si}}^{\text{surf.}} \quad (4)$$

223 where $\dot{n}_{\text{Si}}^{\text{surf.}}$ and $\dot{n}_{\text{Si}}^{\text{ins.}}$ are the reduction rate along the surface and from the surface to the core,
224 respectively. Since the reduction from the surface to the core is much slower than the reduction
225 along the surface after electrolysis of small time t , only the latter is considered. As illustrated in
226 Figure 8(b-2), the Si shell with a thickness of δ and the center of the granule form a spherical sector

227 ACD, the cone angle of which is 2θ ($0 < \theta < \frac{\pi}{2}$). The area of the reduction interface ($A_{inter.}^{small t}$) can

228 be calculated as the difference of the lateral area between the spherical sectors ACD and ABE.

$$229 \quad A_{inter.}^{small t} = \pi r_0^2 \sin \theta - \pi (r_0 - \delta)^2 \sin \theta = \pi [r_0^2 - (r_0 - \delta)^2] \sin \theta \quad (5)$$

230 The reduction rate at small t ($\dot{n}_{Si}^{small t}$) can be described as

$$231 \quad \dot{n}_{Si}^{small t} = \frac{\dot{n}_{O^{2-}}^{small t}}{2} = \frac{-N_I \pi}{2} [r_0^2 - (r_0 - \delta)^2] \sin \theta \cdot D_{surf.} \left(\frac{dC_{O^{2-}}}{dr} \right)_{surf.} \quad (6)$$

232 where $\dot{n}_{O^{2-}}^{small t}$ is the formation rate of O^{2-} ions after electrolysis of small time t . Since the volume

233 difference between the spherical sectors ACD and ABE is regarded as the volume of the reduced

234 part of a single SiO_2 granule ($\Delta V_{SiO_2}^{small t}$), given as

$$235 \quad \Delta V_{SiO_2}^{small t} = \frac{2}{3} \pi r_0^3 (1 - \cos \theta) - \frac{2}{3} \pi (r_0 - \delta)^3 (1 - \cos \theta) = \frac{2}{3} \pi [r_0^3 - (r_0 - \delta)^3] (1 - \cos \theta) \quad (7)$$

236 the reduction rate can also be calculated by

$$\begin{aligned} \dot{n}_{Si}^{small t} &= \frac{dn_{Si}}{dt} = \frac{d \frac{\rho_{SiO_2} N_I \Delta V_{SiO_2}^{small t}}{M_{SiO_2}}}{dt} = \frac{2 \rho_{SiO_2} N_I \pi d \{ [r_0^3 - (r_0 - \delta)^3] (1 - \cos \theta) \}}{3 M_{SiO_2} dt} \\ 237 \quad &= \frac{2 \rho_{SiO_2} N_I \pi}{3 M_{SiO_2}} [r_0^3 - (r_0 - \delta)^3] \sin \theta \frac{d\theta}{dt} \quad (8) \end{aligned}$$

238 where n_{Si} is the number of moles of the reduced Si, ρ_{SiO_2} and M_{SiO_2} are the density and molar weight of

239 SiO_2 , respectively. Combining Eqs. [6] and [8] gives

$$240 \quad \frac{d\theta}{dt} = \frac{-3 M_{SiO_2} [2r_0 - \delta]}{4 \rho_{SiO_2} [3r_0^2 - 3r_0 \delta + \delta^2]} D_{surf.} \left(\frac{dC_{O^{2-}}}{dr} \right)_{surf.} \approx - \frac{M_{SiO_2}}{2 \rho_{SiO_2} r_0} D_{surf.} \left(\frac{dC_{O^{2-}}}{dr} \right)_{surf.} \quad (9)$$

241 The solution of Eq. [9] with the boundary condition $\theta = 0$ when $t = 0$ gives

$$242 \quad \theta = \frac{-M_{SiO_2} t}{2 \rho_{SiO_2} r_0} D_{surf.} \left(\frac{dC_{O^{2-}}}{dr} \right)_{surf.} \quad (10)$$

243 The substitution of Eq. [10] into Eq. [6] gives

$$\begin{aligned} \dot{n}_{O^{2-}}^{small\ t} &= -\frac{A_{plate}}{r_0^2} [2r_0\delta - \delta^2] \sin \left[\frac{-M_{SiO_2}t}{2\rho_{SiO_2}r_0} D_{surf.} \left(\frac{dC_{O^{2-}}}{dr} \right)_{surf.} \right] \cdot D_{surf.} \left(\frac{dC_{O^{2-}}}{dr} \right)_{surf.} \\ &\approx -\frac{2\delta A_{plate} D_{surf.} \left(\frac{dC_{O^{2-}}}{dr} \right)_{surf.}}{r_0} \sin \left[\frac{-M_{SiO_2}t}{2\rho_{SiO_2}r_0} D_{surf.} \left(\frac{dC_{O^{2-}}}{dr} \right)_{surf.} \right] \end{aligned} \quad (11)$$

Equation [11] clearly indicates that reduction rate after electrolysis of small time t decreases with increasing granule radius. It is also understood from Eq. [11] that the reduction rate at the beginning of electrolysis would increase with increasing time t . Even though this tendency is not clearly observed in the current experiments because the amount of SiO_2 granules is too small (0.13 g), it was presented in previous experiments on a larger scale (more than 10 g of SiO_2 granules).^[69]

After electrolysis of large time t , a core (SiO_2)–shell (Si) structure forms for all granules, as shown in Figure 8(c-1). At this moment, the whole granule surface is reduced, and thus only the reduction from the surface to the core continues. The reaction interface is the surface of the unreacted SiO_2 core. The reduction rate ($\dot{n}_{Si}^{large\ t}$) can be calculated as

$$\dot{n}_{Si}^{large\ t} = \frac{\dot{n}_{O^{2-}}^{large\ t}}{2} = -2\pi r_i^2 N_{II} D_{ins.} \left(\frac{dC_{O^{2-}}}{dr} \right)_{ins.} \quad (12)$$

where $\dot{n}_{O^{2-}}^{large\ t}$ is the formation rate of O^{2-} ions after electrolysis of large time t , r_i is the radius of the unreduced SiO_2 core as shown in Figure 8(c-2), N_{II} is the number of granules reduced after large time t , and $D_{ins.}$ and $\left(\frac{dC_{O^{2-}}}{dr} \right)_{ins.}$ are the diffusion coefficient and concentration gradient of O^{2-} ions in $CaCl_2$ in the crevices of the porous Si shells, respectively. Assuming a linear concentration gradient of O^{2-} ions, $\left(\frac{dC_{O^{2-}}}{dr} \right)_{ins.} = \frac{C_0 - C_i}{r_0 - r_i}$, where C_0 and C_i are the concentrations of O^{2-} ions at the outer and inner surfaces of the Si shell, respectively, Eq. [12] becomes

$$\dot{n}_{Si}^{large\ t} = 2\pi r_i^2 N_{II} D_{ins.} \frac{C_i - C_0}{r_0 - r_i} \quad (13)$$

Since the volume of the reduced part of a single SiO_2 granule ($\Delta V_{SiO_2}^{large\ t}$) can be calculated as

$$\Delta V_{SiO_2}^{large\ t} = \frac{4}{3}\pi r_0^3 - \frac{4}{3}\pi r_i^3 \quad (14)$$

the reduction rate can also be described by

$$\dot{n}_{Si}^{large\ t} = \frac{dn_{Si}}{dt} = \frac{\frac{\rho_{SiO_2} N_{II} \Delta V_{SiO_2}^{large\ t}}{M_{SiO_2}}}{dt} = \frac{-4\rho_{SiO_2} N_{II} \pi r_i^2}{M_{SiO_2}} \frac{dr_i}{dt} \quad (15)$$

Combining Eqs. [13] and [15] yields

$$\frac{2(r_i - r_0)dr_i}{dt} = \frac{(C_i - C_0)D_{ins.}M_{SiO_2}}{\rho_{SiO_2}} \quad (16)$$

Assuming $D_{ins.}$, C_0 , and C_i are independent of time, the solution of Eq. [16] with the boundary

condition $r_i = r_0$ when $t = 0$ gives

$$(r_0 - r_i)^2 = \frac{(C_i - C_0)D_{ins.}M_{SiO_2}}{\rho_{SiO_2}} t \quad (17)$$

Since the granule number can be described as

$$N_{II} = \frac{\frac{W_{SiO_2}}{\rho_{SiO_2}}}{\frac{4}{3}\pi r_0^3} = \frac{3W_{SiO_2}}{4\rho_{SiO_2}\pi r_0^3} \quad (18)$$

where W_{SiO_2} is the total weight of SiO_2 , the substitution of Eqs. [17] and [18] into Eq. [13] yields

$$\dot{n}_{Si}^{large\ t} = \left[r_0 - \sqrt{\frac{(C_i - C_0)D_{ins.}M_{SiO_2}}{\rho_{SiO_2}}} t \right]^2 \frac{3W_{SiO_2}}{2r_0^3} \sqrt{\frac{(C_i - C_0)D_{ins.}}{M_{SiO_2}\rho_{SiO_2}t}} \quad (19)$$

Equation [19] is a monotonically decreasing function of r_0 , which indicates that the reduction rate at

an electrolysis time of large t decreases with increasing granule radius. Moreover, the reduction rate

also decreases with increasing electrolysis time. These tendencies are in accordance with the

experimental results shown in Figure 6.

279 **C. Apparent Current Density**

280 Based on the current transient curves during electrolysis (Figure 6), the apparent current density
281 was evaluated. In the case of the blank test without charging with SiO₂ granules, only the current
282 (I_{blank}) contributed by the side electrochemical reactions (I_{side}) is obtained

$$283 \quad I_{\text{blank}} = I_{\text{side}} \quad (20)$$

284 For the electrolysis after charging with SiO₂ granules, the overall current (I_{all}) is the result of both the
285 SiO₂ reduction (I_{SiO_2}) and the side reactions.

$$286 \quad I_{\text{all}} = I_{\text{SiO}_2} + I_{\text{side}} \quad (21)$$

287 Assuming the current corresponding to side reactions is independent of the electrolysis time and
288 charge of SiO₂ granules, the apparent current density corresponding to SiO₂ reduction (i_{SiO_2}) can be
289 calculated by

$$290 \quad i_{\text{SiO}_2} = \frac{I_{\text{SiO}_2}}{A_{\text{plate}}} = \frac{I_{\text{all}} - I_{\text{blank}}}{A_{\text{plate}}} \quad (22)$$

291 Using the data in Figure 6 and taking $I_{\text{side}} \equiv 0.05A$, the apparent current densities during
292 electrolysis for 20 min using SiO₂ granules with various size ranges were calculated and the results
293 are shown in Figure 9. It is clear that the current density gradually decreases with increasing
294 electrolysis time and that smaller SiO₂ granules results in a larger current density. In the case of
295 using SiO₂ granules less than 0.1 mm in size, electrolysis within 20 min maintained a current density
296 of no less than 0.4 A cm⁻². This result basically agrees with those of a previous study, in which the

297 current density was obtained by calculating from the weight change of the sample before and after
 298 electrolysis.^[70] These results indicate that the productivity would be improved by using fine SiO₂
 299 granules as the raw materials for a new SOG-Si production process in the future.

300 ***** Figure 9 *****

301

302 IV. CONCLUSIONS

303 The effect of granule size on the kinetics of electrochemical reduction of SiO₂ granules in molten
 304 CaCl₂ at 1123 K (850 °C) was clarified. Fine SiO₂ granules are favorable for a high reduction rate by
 305 lowering the contact potential drop between the bottom Si plate and the reduced Si. The use of fine
 306 granules also improves the diffusion of O²⁻ ions in CaCl₂ inside the porous Si shell formed on the
 307 SiO₂ core. The electrolysis using SiO₂ granules less than 0.1 mm in size maintained a current density
 308 of no less than 0.4 A cm⁻² within 20 min, indicating that electrochemical reduction of fine SiO₂
 309 granules in molten CaCl₂ has the potential to become a high-yield solar-grade silicon production
 310 process.

311 ACKNOWLEDGMENTS

312 This study was partly supported by Core Research for Evolutionary Science and Technology

313 (CREST), Japan Science and Technology Agency (JST) and Grants-in-Aid for Scientific Research A

314 from the Japan Society for the Promotion of Science (JSPS).

315

316

317

NOMENCLATURE

$A_{\text{cont.}}$	Effective area for each contact point between SiO_2 granules and the Si plate
A_{plate}	Geometrical area of the bottom Si plate
$A_{\text{inter.}}^{\text{small } t}$	Area of the reduction interface after electrolysis of small time t
C_i	Concentration of O^{2-} ions at the inner surface of the Si shell of the partly reduced SiO_2 granules after electrolysis of large time t
C_0	Concentration of O^{2-} ions at the outer surface of the Si shell of the partly reduced SiO_2 granules after electrolysis of large time t
$D_{\text{ins.}}$	Diffusion coefficient of O^{2-} ions in CaCl_2 in the crevice of the porous Si shell of the partly reduced SiO_2 granules after electrolysis of large time t
$D_{\text{surf.}}$	Diffusion coefficient of O^{2-} ions in CaCl_2 at the SiO_2 granule surface
$\left(\frac{dC_{\text{O}^{2-}}}{dr}\right)_{\text{ins.}}$	Concentration gradient of O^{2-} ions in CaCl_2 in the crevice of the porous Si shell of the partly reduced SiO_2 granules after electrolysis of large time t
$\left(\frac{dC_{\text{O}^{2-}}}{dr}\right)_{\text{surf.}}$	Concentration gradient of O^{2-} ions in CaCl_2 at the SiO_2 granule surface
I_{all}	Current obtained in the case of a test with charging SiO_2
I_{blank}	Current obtained in the case of a blank test without charging SiO_2
I_{side}	Current contributed by the side electrochemical reactions
I_{SiO_2}	Current contributed by SiO_2 reduction
i_{SiO_2}	Apparent current density corresponding to SiO_2 reduction
M_{SiO_2}	Molar weight of SiO_2
N_{I}	Number of SiO_2 granules directly neighboring the Si plate
N_{II}	Total number of SiO_2 granules
n_{Si}	Number of moles of the reduced Si
$\dot{n}_{\text{Si}}^{t \rightarrow 0}$	Reduction rate of SiO_2 granules at the start moment of the electrolysis
$\dot{n}_{\text{Si}}^{\text{overall}}$	Overall reduction rate of SiO_2 granules
$\dot{n}_{\text{Si}}^{\text{surf.}}$	Reduction rate of SiO_2 granules along surface
$\dot{n}_{\text{Si}}^{\text{ins.}}$	Reduction rate of SiO_2 granules from surface to core
$\dot{n}_{\text{Si}}^{\text{ins.}}$	Reduction rate of SiO_2 granules after electrolysis of small time t
$\dot{n}_{\text{Si}}^{\text{small } t}$	Reduction rate of SiO_2 granules after electrolysis of large time t
$\dot{n}_{\text{Si}}^{\text{large } t}$	Formation rate of O^{2-} ions at the start moment of the electrolysis
$\dot{n}_{\text{Si}}^{\text{large } t}$	Formation rate of O^{2-} ions after electrolysis of small time t
$\dot{n}_{\text{O}^{2-}}^{t \rightarrow 0}$	Formation rate of O^{2-} ions after electrolysis of large time t
$\dot{n}_{\text{O}^{2-}}^{\text{small } t}$	Radius of the SiO_2 granule in Figure 8(b-2)
$\dot{n}_{\text{O}^{2-}}^{\text{large } t}$	Radius of the unreduced core of the partly reduced SiO_2 granule in Figure 8(c-2)
r_0	Electrolysis time
r_i	Volume of the reduced part of a SiO_2 granule after electrolysis of small time t
t	Volume of the reduced part of a SiO_2 granule after electrolysis of large time t
$\Delta V_{\text{SiO}_2}^{\text{small } t}$	Total weight of SiO_2 granules
	Thickness of the reduced Si shell after electrolysis of small time t in Figure 8(b-2)

$\Delta V_{SiO_2}^{large\ t}$ Half of the cone angle of the spherical sector ACD in Figure 8(b-2)
 W_{SiO_2} Density of SiO_2
 δ
 θ
 ρ_{SiO_2}

318

319

320

321

322

REFERENCES

323

1. European Photovoltaic Industry Association: *Market Report 2013*, European Photovoltaic

324

Industry Association, Brussels, March, 2014.

325

2. Observ'ER: *Fifteenth Inventory 2013 Edition—Worldwide Electricity Production from*

326

Renewable Energy Sources, Observ'ER, Paris, June, 2013.

327

3. German Advisory Council on Global Change: *World in Transition—Towards Sustainable*

328

Energy Systems, Earthscan, London, 2003.

329

4. Arumu Publishing Co.: *Rare Metal News*, Arumu Publishing Co., Tokyo, August, 2014.

330

5. Arumu Publishing Co.: *Rare Metal News*, Arumu Publishing Co., Tokyo, April, 2014.

331

6. H. Schweickert, K. Reuschel, and H. Gutsche: U.S. patent, US3,011,877, 1961.

332

7. H. Gutsche: U.S. patent, US3,042,494, 1962.

333

8. G. Bye and B. Ceccaroli: *Sol. Energy Mater. Sol. Cells*, 2014, vol. 130, pp.634-46.

334

9. H. W. Ling: U.S. Patent, US3,012,861, 1961.

335

10. L. Bertrand, N. Star, and C. M. Olson: U.S. Patent, US3,012,862, 1961.

- 336 11. K. Morita and T. Miki: *Intermetallics*, 2003, vol. 11, pp. 1111–17.
- 337 12. V. Hoffmann, K. Petter, J. Djordjevic-Reiss, E. Enebakk, J. T. Håkedal, R. Tronstad, T.
- 338 Vlasenko, I. Buchovskaja, S. Beringov, and M. Bauer: *Proc. 23rd EU PVSEC*, Valencia, Spain,
- 339 1-5 Sept. 2008, pp. 1117–20.
- 340 13. Y. V. Meteleva-Fischer, Y. Yang, R. Boom, B. Kraaijveld and H. Kuntzel: *JOM*, 2012, vol. 64,
- 341 pp. 957–967.
- 342 14. IHS Technology: *PV Manufacturing Technology Report - 2014*, IHS Technology, El Segundo
- 343 Feb., 2014.
- 344 15. S. Wakamatsu and H. Oda: PCT International Patent, WO2001/085613, 2001.
- 345 16. A. Sjøiland, M. G. Dolmen, J. Heide, U. Thisted, G. Halvorsen, G. Ausland, K. Friestad, P.
- 346 Preis, K. Peter, O. Graf, T. Bartel, and R. Tronstad: *Sol. Energy Mater. Sol. Cells*, 2014, vol.
- 347 130, pp. 661–67.
- 348 17. K. Yasuda, K. Morita, and T. H. Okabe: *Energy Technology*, 2014, vol. 2, pp. 141–54.
- 349 18. W. O. Filtvedt, M. Javidi, A. Holt, M. C. Melaaen, E. Marstein, H. Tathgar, and P. A.
- 350 Ramachandran: *Sol. Energy Mater. Sol. Cells*, 2010, vol. 94, pp. 1980–95.
- 351 19. B. G. Gribov and K. V. Zinov'ev: *Inorg. Mater.*, 2003, vol. 39, pp. 653–62.
- 352 20. H. Oda: *Kogyo Zairyo*, 2007, vol. 55, pp. 30–34.
- 353 21. A. F. B. Braga, S. P. Moreira, P. R. Zampieri, J. M. G. Bacchin, and P. R. Mei: *Sol. Energy*

- 354 *Mater. Sol. Cells*, 2008, vol. 92, pp. 418–24.
- 355 22. M. D. Johnston, L. T. Khajavi, M. Li, S. Sokhanvaran, and M. Barati, *JOM*, 2012, vol. 64, pp.
- 356 935–45.
- 357 23. Y. Sakaguchi, M. Ishizaki, T. Kawahara, M. Fukai, M. Yoshiyagawa, and F. Aratani, *ISIJ Int.*,
- 358 1992, vol. 32, pp. 643–49.
- 359 24. K. Suzuki, T. Kumagai, and N. Sano: *ISIJ Int.*, 1992, vol. 32, pp. 630–34.
- 360 25. T. Ikeda and M. Maeda: *ISIJ Int.*, 1992, vol. 32, pp. 635–42.
- 361 26. J. C. S. Pires, J. Otubo, A. F. B. Braga, and P. R. Mei: *J. Mater. Processing Tech.* 2005, vol.
- 362 169, pp. 16–20.
- 363 27. J. L. Gumaste, B. C. Mohanty, R. K. Galgali, U. Syamaprasad, B. Nayak, S. K. Singh, and P. K.
- 364 Jena: *Sol. Energy Mater.*, 1987, vol. 16, pp. 289–96.
- 365 28. T. Yoshikawa and K. Morita: *JOM*, 2012, vol. 64, pp. 946–51.
- 366 29. I. C. Santos, A. P. Goncalves, C. S. Santos, M. Almeida, M. H. Afonso, and M. J. Cruz:
- 367 *Hydrometallurgy*, 1990, vol. 23, pp. 237–246.
- 368 30. Y. Sun, Q. Ye, C. Guo, H. Chen, X. Lang, F. David, Q. Luo, and C. Yang: *Hydrometallurgy*,
- 369 2013, vol. 139, pp. 64–72.
- 370 31. J. Safarian and M. Tangstad: *Metall. Mater. Trans. B*, 2012, vol. 43, pp. 1427–45.
- 371 32. M. A. Martorano, J. B. F. Neto, T. S. Oliveira, and T. O. Tsubaki: *Mater. Sci. Eng. B*, 2011, vol.

- 372 176, pp. 217–26.
- 373 33. S. Honda, M. Yasueda, S. Hayashida, and M. Yamaguchi: Japanese Patent Application,
374 JP2007145663, 2007.
- 375 34. K. Saegusa and T. Yamabayashi: PCT International Patent WO2007/001093, 2007.
- 376 35. K. Yasuda and T. H. Okabe: *JOM*, 2010, vol. 62, pp 94–101.
- 377 36. K. Yasuda, K. Saegusa, and T. H. Okabe: *Metall. Mater. Trans. B*, 2011, vol. 42, pp. 37–49.
- 378 37. E. Robert and T. Zijlema: PCT International Patent WO2006/100114, 2006.
- 379 38. C. Rosenkilde: PCT International Patent WO2008/120994, 2008.
- 380 39. H. Tezuka: PCT International Patent WO2008/153181, 2008.
- 381 40. K. Saito, H. Munakata, and T. Mizoguchi: PCT International Patent WO2011/071030, 2011.
- 382 41. R. Monnier, D. Barakat, and J. Giacometti: U.S. Patent, US3,254,010, 1966.
- 383 42. J. Olson and K. Carleton: *J. Electrochem. Soc.*, 1981, vol. 128, pp. 2698–99.
- 384 43. J. Cai, X. Luo, G. M. Haarberg, O. E. Kongstein, and S. Wang: *J. Electrochem. Soc.*, 2012, vol.
385 159, pp. D155–58.
- 386 44. D. Elwell and R. S. Feigelson: *Sol. Energy Mater.*, 1982, vol. 6, pp. 123–45.
- 387 45. D. Elwell and G. M. Rao: *J. Appl. Electrochem.*, 1988, vol. 18, pp. 15–22.
- 388 46. T. Oishi, M. Watanabe, K. Koyama, M. Tanaka, and K. Saegusa: *J. Electrochem. Soc.*, 2011,
389 vol. 158, pp. E93–99.

- 390 47. J. Xu and G. M. Haarberg: *High Temperature Materials and Processes*, 2013, vol. 32, pp. 97–
- 391 105.
- 392 48. Y. Jiang, J. Xu, X. Guan, U.B. Pal, and S.N. Basu: *MRS Proceedings*, 2013, vol. 1493, pp. 231–
- 393 35.
- 394 49. G. Z. Chen, D. J. Fray, and T. W. Farthing: *Nat.*, 2000, vol. 407, pp. 361-64.
- 395 50. X. Y. Yan and D. J. Fray: *Metall. Mater. Trans. B*, 2002, vol. 33, pp. 685–93.
- 396 51. G. Z. Chen, E. Gordo, and D. J. Fray: *Metall. Mater. Trans. B*, 2004, vol. 35, pp. 223–33.
- 397 52. K. S. Mohandas and D. J. Fray: *Metall. Mater. Trans. B*, 2009, vol. 40, pp. 685–99.
- 398 53. X. Y. Yan and D. J. Fray: *J. Appl. Electrochem.*, 2009, vol. 39, pp. 1349–60.
- 399 54. Q. Song, Q. Xu, X. Kang, J. Du, and Z. Xi: *J. Alloy. Compd.*, 2010, vol. 490, pp. 241–46.
- 400 55. M. Erdoğan and I. Karakaya: *Metall. Mater. Trans. B*, 2010, vol. 41, pp. 798–804.
- 401 56. A. M. Abdelkader and D. J. Fray: *Electrochim. Acta*, 2012, vol. 64, pp. 10-16.
- 402 57. W. Xiao and D. Wang: *Chem. Soc. Rev.*, 2014, vol. 43, pp. 3215-28.
- 403 58. T. Nohira, K. Yasuda, and Y. Ito: *Nat. Mater.*, 2003, vol. 2, pp. 397–401.
- 404 59. K. Yasuda, T. Nohira, K. Amezawa, Y. H. Ogata, and Y. Ito: *J. Electrochem. Soc.*, 2005, vol.
- 405 152, pp. D69–74.
- 406 60. K. Yasuda, T. Nohira, Y. H. Ogata, and Y. Ito: *Electrochim. Acta*, 2005, vol. 51, pp. 561–65.
- 407 61. K. Yasuda, T. Nohira, and Y. Ito: *J. Phys. Chem. Solids*, 2005, vol. 66, pp. 443–47.

- 408 **62.** K. Yasuda, T. Nohira, Y. H. Ogata, and Y. Ito: *J. Electrochem. Soc.*, 2005, vol. 152, pp. D208–
409 12.
- 410 **63.** K. Yasuda, T. Nohira, R. Hagiwara, and Y. H. Ogata: *J. Electrochem. Soc.*, 2007, vol. 154, pp.
411 E95–E101.
- 412 **64.** K. Yasuda, T. Nohira, R. Hagiwara, and Y. H. Ogata: *Electrochim. Acta.*, 2007, vol. 53, pp.
413 106–10.
- 414 **65.** K. Yasuda, T. Nohira, K. Takahashi, R. Hagiwara, and Y. H. Ogata: *J. Electrochem. Soc.*, 2005,
415 vol. 152, pp. D232–37.
- 416 **66.** Y. Nishimura, T. Nohira, K. Yasuda, Y. Fukunaka, and R. Hagiwara: *Trans. Mater. Res. Soc.*
417 *Jpn.*, 2010, vol. 35, pp. 47-49.
- 418 **67.** Y. Nishimura, T. Nohira, K. Kobayashi, and R. Hagiwara: *J. Electrochem. Soc.*, 2011, vol.158,
419 pp. E55–59.
- 420 **68.** K. Yasuda, T. Nohira, K. Kobayashi, N. Kani, T. Tsuda, and R. Hagiwara: *Energy Technology*,
421 2013, vol. 1, pp. 245–52.
- 422 **69.** T. Toba, K. Yasuda, T. Nohira, X. Yang, R. Hagiwara, K. Ichitsubo, K. Masuda, and T.
423 Homma: *Electrochemistry*, 2013, vol. 81, pp. 559–65.
- 424 **70.** X. Yang, K. Yasuda, T. Nohira, R. Hagiwara, and T. Homma: *J. Electrochem. Soc.*, 2014, vol.
425 161, pp. D3116–19.

- 426 71. X. Yang, K. Yasuda, T. Nohira, R. Hagiwara, and T. Homma: *Metall. Mater. Trans. B*, 2014,
427 vol. 45, pp. 1337-44.
- 428 72. X. Jin, P. Gao, D. Wang, X. Hu, and G. Z. Chen: *Angew. Chem.*, 2004, vol. 116, pp. 751–54.
- 429 73. W. Xiao, X. Jin, Y. Deng, D. Wang, X. Hu, and G. Z. Chen: *ChemPhysChem.*, 2006, vol. 7, pp.
430 1750–58.
- 431 74. W. Xiao, X. Jin, Y. Deng, D. Wang, X. Hu, and G. Z. Chen: *J. Electroanal. Chem.*, 2010, vol.
432 639, pp. 130–40.
- 433 75. W. Xiao, X. Jin, and G. Z. Chen: *J. Mater. Chem. A.*, 2013, vol. 1, pp. 10243–50.
- 434 76. W. Xiao, X. Wang, H. Yin, H. Zhu, X. Mao, and D. Wang: *RSC Advances*, 2012, vol. 2, pp.
435 7588–93.
- 436 77. P. C. Pistorius and D. J. Fray: *J. S. Afr. Inst. Min. Metall.*, 2006, vol. 106, pp. 31–41.
- 437 78. S. Lee, J. Hur, and C. Seo: *J. Ind. Eng. Chem.*, 2008, vol. 14, pp. 651–54.
- 438 79. E. Juzeliunas, A. Cox, and D. J. Fray: *Electrochem. Comm.*, 2010, vol. 12, pp. 1270–74.
- 439 80. E. Ergül, İ. Karakaya, and M. Erdoğan: *J. Alloy. Compd.*, 2011, vol. 509, pp. 899–903.
- 440 81. S. K. Cho, F. F. Fan, and A. J. Bard: *Electrochim. Acta*, 2012, vol. 65, pp. 57–63.
- 441 82. J. Zhao, S. Lu, L. Hu, and C. Li: *J. Energy Chem.*, 2013, vol. 22, pp. 819-25.
- 442 83. J. Zhao, J. Li, P. Ying, W. Zhang, L. Meng, and C. Li: *ChemCom.*, 2013, vol. 49, pp. 4477-79.
- 443 84. H. Nishihara, T. Suzuki, H. Itoi, B. An, S. Iwamura, R. Berenguer, and T. Kyotani: *Nanoscale*,

444 2014, vol. 6, pp. 10574-83.

445 85. G. Olson and J. Roth: *Mater. Sci. Rep.*, 1988, vol. 3, pp. 1-77.

446

Caption list

- 447
- 448 Figure 1—Appearances of the SiO_2 granules with size ranges of (a) less than 0.1 mm, (b) 0.10–0.25
- 449 mm, (c) 0.5–1.0 mm and (d) 1.0–2.0 mm.
- 450 Figure 2—A schematic of (a) the electrolysis cell and (b) the working electrode.
- 451 Figure 3—Appearances of the upper surface of the bottom Si plate after electrolysis using SiO_2
- 452 granules with size ranges of (a) less than 0.1 mm, (b) 0.10–0.25 mm, (c) 0.5–1.0 mm, (d)
- 453 1.0–2.0 mm for 10 min and (e) a blank electrolysis test for 10 min at 0.5 V vs. Ca^{2+}/Ca in
- 454 molten CaCl_2 at 1123 K (850 °C).
- 455 Figure 4—Cross sections of the working electrodes using SiO_2 granules with size ranges of (a) less
- 456 than 0.1 mm, (b) 0.10–0.25 mm, (c) 0.5–1.0 mm and (d) 1.0–2.0 mm after electrolysis for
- 457 (I) 20 min and (II) 60 min at 0.5 V vs. Ca^{2+}/Ca in molten CaCl_2 at 1123 K (850 °C).
- 458 Figure 5—Thickness of the reduced layers after electrolysis for 20, 60 and 100 min using SiO_2
- 459 granules with different size ranges at 0.5 V vs. Ca^{2+}/Ca in molten CaCl_2 at 1123 K
- 460 (850 °C).
- 461 Figure 6—Current transient curves during electrolysis using SiO_2 granules with size ranges of (a)
- 462 less than 0.1 mm, (b) 0.10–0.25 mm, (c) 0.5–1.0 mm and (d) 1.0–2.0 mm for 20 min and
- 463 (e) during a blank electrolysis test for 10 min at 0.5 V vs. Ca^{2+}/Ca in molten CaCl_2 at 1123
- 464 K (850 °C).
- 465 Figure 7—Schematics of the contact between SiO_2 granules and the bottom current collector (Si
- 466 plate).
- 467 Figure 8—Schematics of the reduction of the SiO_2 granules during electrolysis.
- 468 Figure 9—Variation of apparent current density during electrolysis within 20 min using SiO_2
- 469 granules with size ranges of (a) less than 0.1 mm, (b) 0.10–0.25 mm, (c) 0.5–1.0 mm and
- 470 (d) 1.0–2.0 mm at 0.5 V vs. Ca^{2+}/Ca in molten CaCl_2 at 1123 K (850 °C).

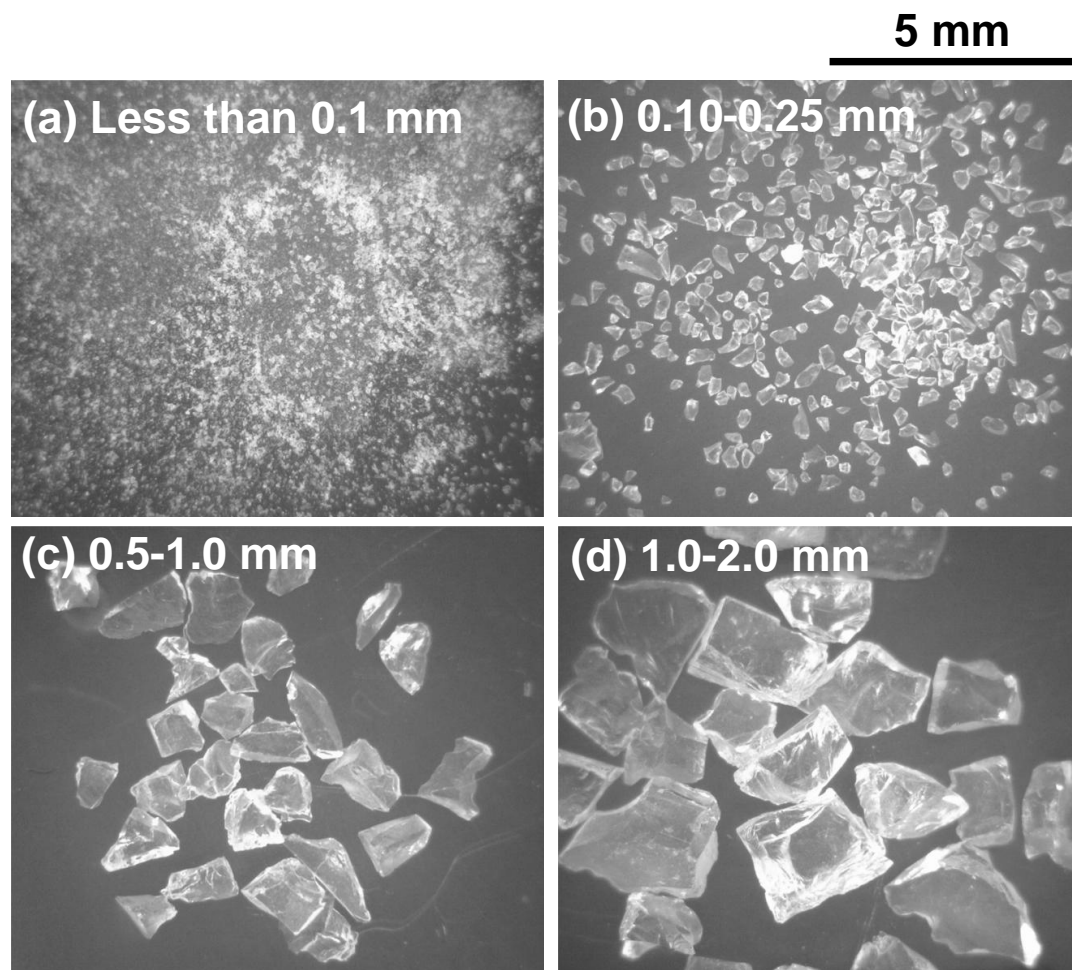


Figure 1—Appearances of the SiO_2 granules with size ranges of (a) less than 0.1 mm, (b) 0.10–0.25 mm, (c) 0.5–1.0 mm and (d) 1.0–2.0 mm.

Yang et al.

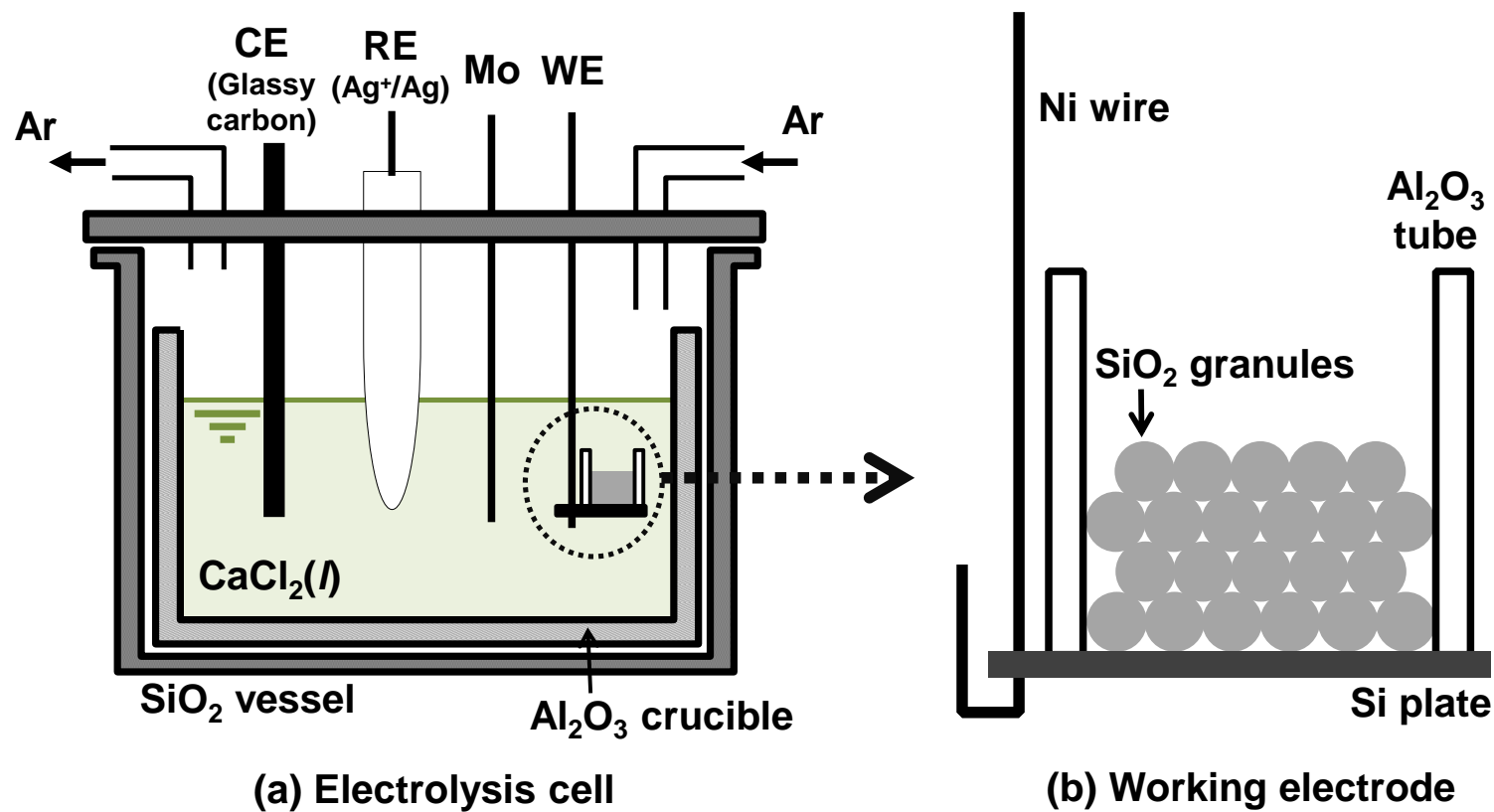


Figure 2—A schematic of (a) the electrolysis cell and (b) the working electrode.

Yang et al.

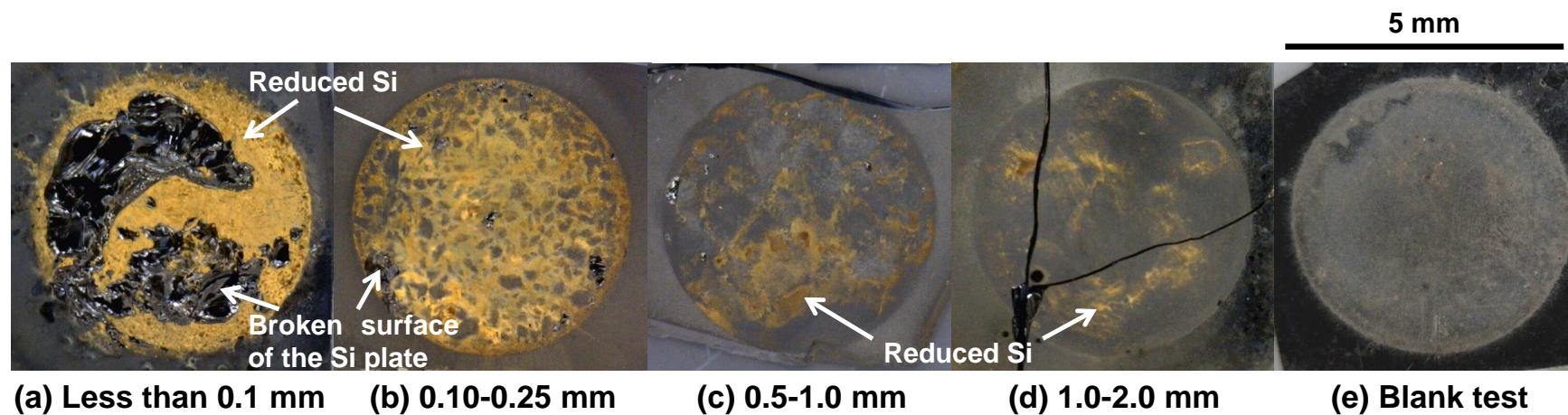


Figure 3—Appearances of the upper surface of the bottom Si plate after electrolysis using SiO_2 granules with size ranges of (a) less than 0.1 mm, (b) 0.10–0.25 mm, (c) 0.5–1.0 mm, (d) 1.0–2.0 mm for 10 min and (e) a blank electrolysis test for 10 min at 0.5 V vs. Ca^{2+}/Ca in molten CaCl_2 at 1123 K (850 °C).

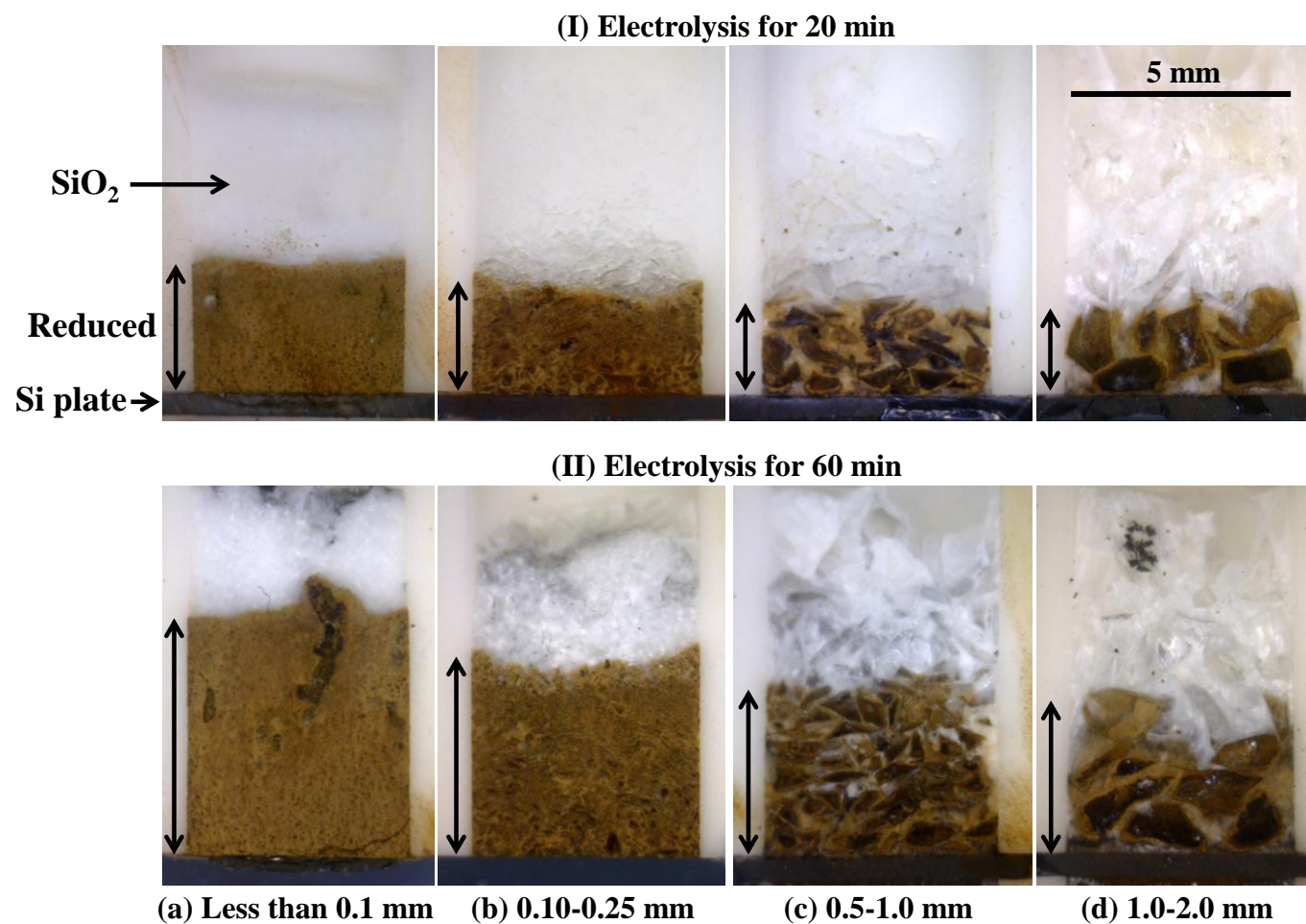


Figure 4—Cross sections of the working electrodes using SiO_2 granules with size ranges of (a) less than 0.1 mm, (b) 0.10–0.25 mm, (c) 0.5–1.0 mm and (d) 1.0–2.0 mm after electrolysis for (I) 20 min and (II) 60 min at 0.5 V vs. Ca^{2+}/Ca in molten CaCl_2 at 1123 K (850 °C).

Yang et al.

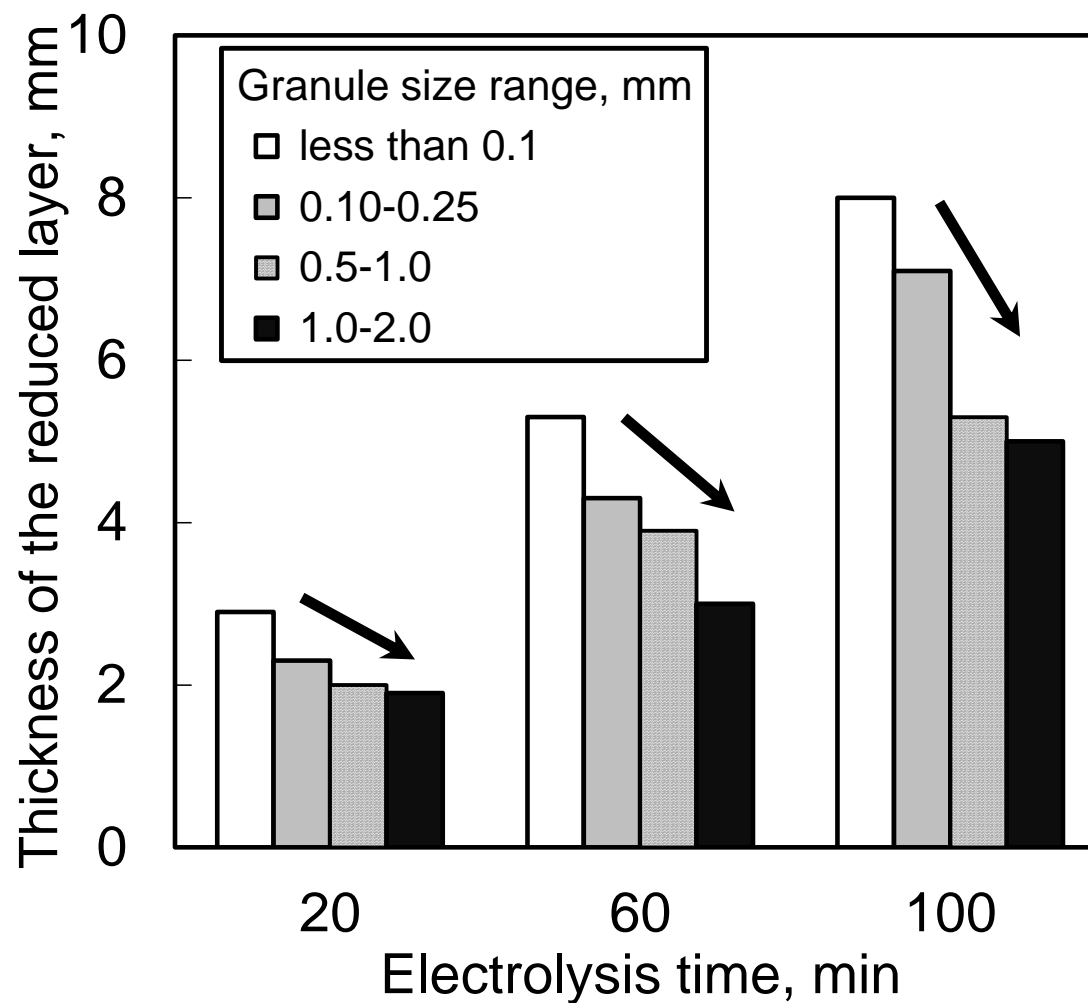


Figure 5—Thickness of the reduced layers after electrolysis for 20, 60 and 100 min using SiO₂ granules with different size ranges at 0.5 V vs. Ca²⁺/Ca in molten CaCl₂ at 1123 K (850 °C).

Yang et al.

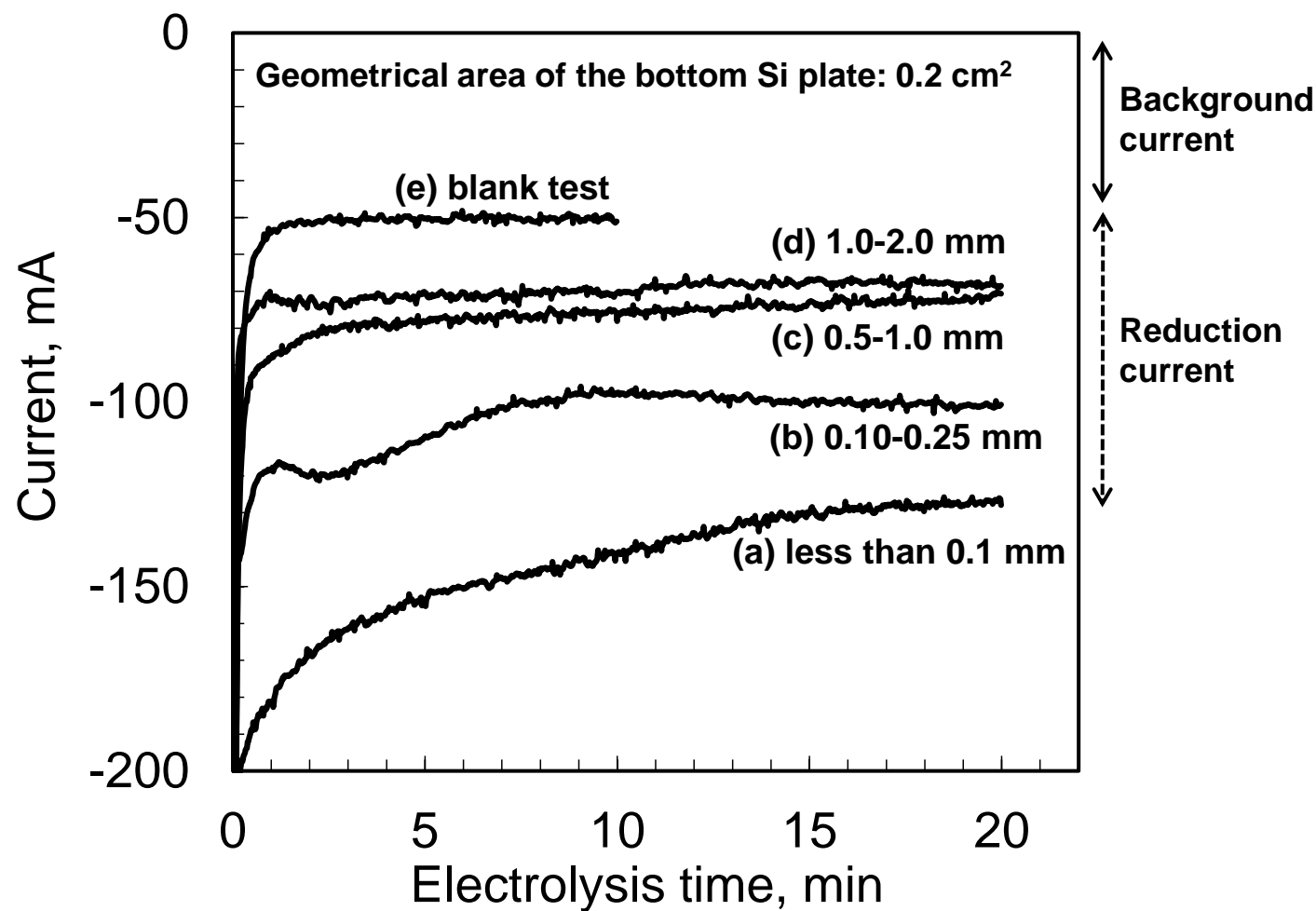


Figure 6—Current transient curves during electrolysis using SiO₂ granules with size ranges of (a) less than 0.1 mm, (b) 0.10–0.25 mm, (c) 0.5–1.0 mm and (d) 1.0–2.0 mm for 20 min and (e) during a blank electrolysis test for 10 min at 0.5 V vs. Ca²⁺/Ca in molten CaCl₂ at 1123 K (850 °C).

Yang et al.

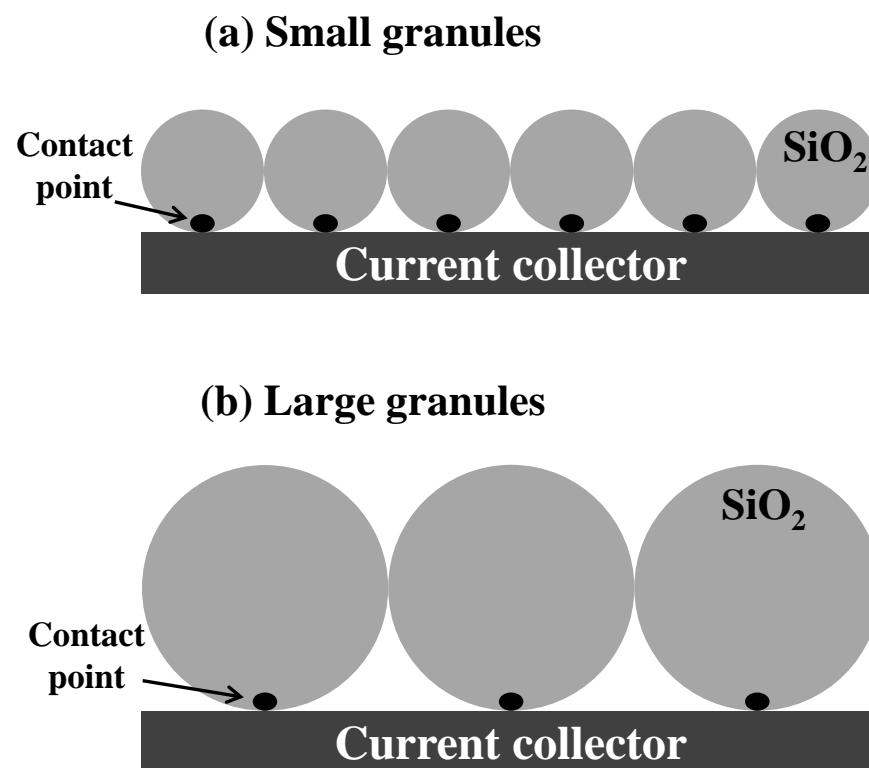


Figure 7—Schematics of the contact between SiO₂ granules and the bottom current collector (Si plate).

Yang et al.

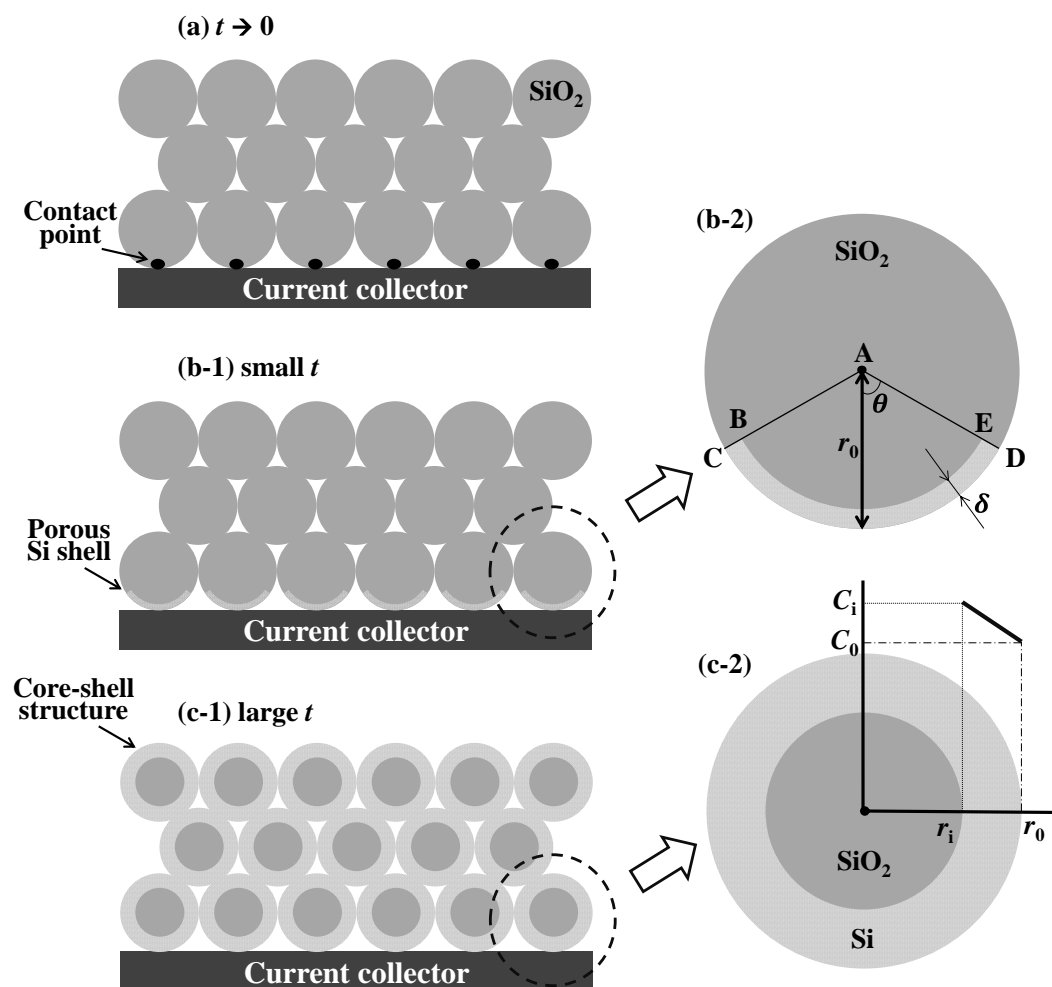


Figure 8—Schematics of the reduction of the SiO_2 granules during electrolysis.

Yang et al.

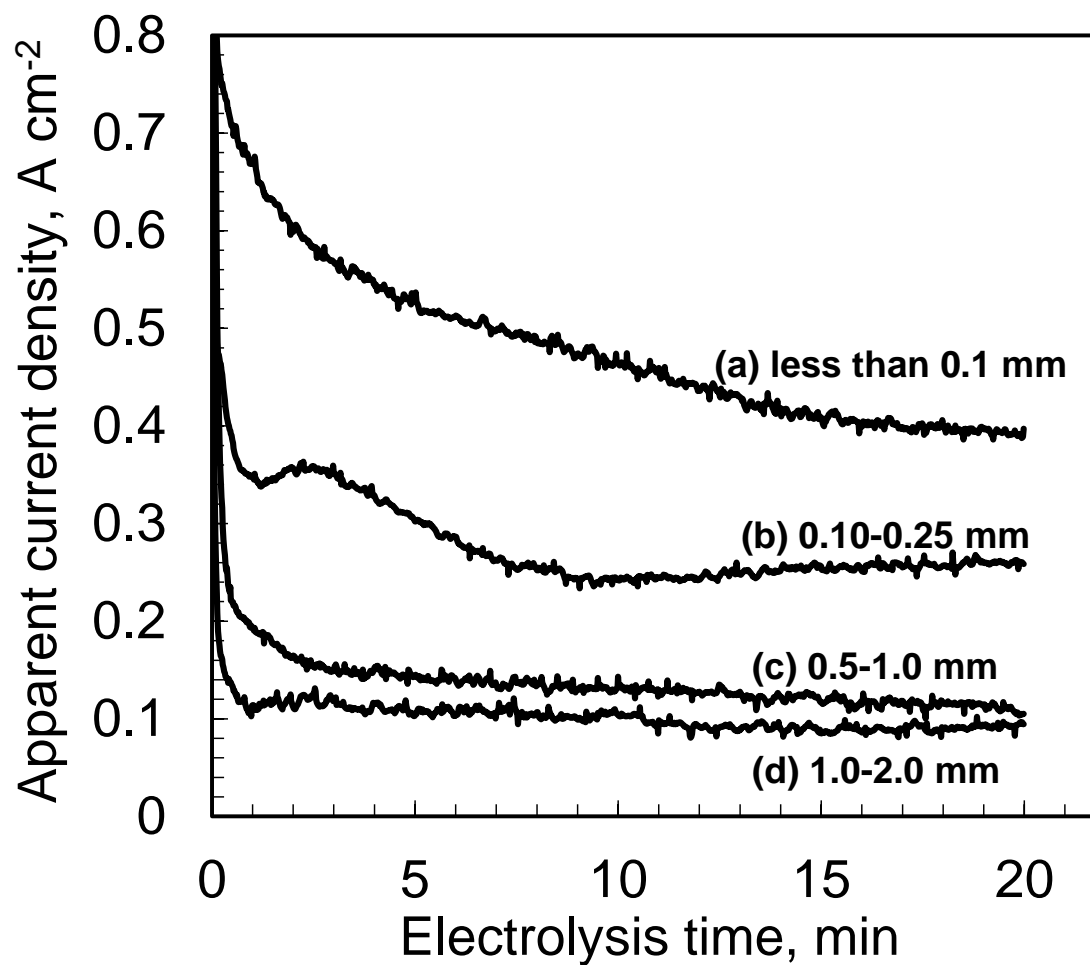


Figure 9—Variation of apparent current density during electrolysis within 20 min using SiO₂ granules with size ranges of (a) less than 0.1 mm, (b) 0.10–0.25 mm, (c) 0.5–1.0 mm and (d) 1.0–2.0 mm at 0.5 V vs. Ca²⁺/Ca in molten CaCl₂ at 1123 K (850 °C).

Yang et al.